

ACCEPTED MANUSCRIPT

This is an early electronic version of an as-received manuscript that has been accepted for publication in the Journal of the Serbian Chemical Society but has not yet been subjected to the editing process and publishing procedure applied by the JSCS Editorial Office.

Please cite this article as H. Koyuncu and A. R. Kul, *J. Serb. Chem. Soc.* (2023) <https://doi.org/10.2298/JSC23053089K>

This “raw” version of the manuscript is being provided to the authors and readers for their technical service. It must be stressed that the manuscript still has to be subjected to copyediting, typesetting, English grammar and syntax corrections, professional editing, and authors’ review of the galley proof before it is published in its final form. Please note that during these publishing processes, many errors may emerge which could affect the final content of the manuscript and all legal disclaimers applied according to the policies of the Journal.



J. Serb. Chem. Soc. **00(0)**1-16 (2023)
JSCS-12417

Investigation of the adsorption behaviors of thymol blue, crystal violet, and rhodamine b on lichen-derived activated carbon

HÜLYA KOYUNCU^{1*} and ALİ RIZA KUL²

¹Bursa Technical University, Faculty of Engineering and Natural Sciences, Chemical Engineering Department, 16310, Bursa, Türkiye, and ²Van Yüzyüncü Yıl University, Faculty of Science, Chemistry Department, 65080, Van, Türkiye.

(Received 30 May; Revised 10 August; Accepted 20 November 2023)

Abstract: Since thymol blue (TB), crystal violet (CV), and rhodamine b (RB) are frequently used in various industries, they cause environmental pollution owing to the process wastewater. The current study focused on the removal of TB, CV, and RB from aqueous media with lichen-derived activated carbon (LDAC) and comparing their adsorption behavior. The maximum Langmuir adsorption capacity for TB, CV, and RB was found to be 400 mg g⁻¹, 212.766 mg g⁻¹, and 344.828 mg g⁻¹, respectively. The removal (%) of TB, CV, and RB was found to be 86.38 %, 79.02 %, and 82.73 % at the same conditions, respectively. Experimental data were interpreted with some commonly used kinetic and isotherm models. Calculated activation energies, D-R model energies, enthalpy values, and evaluation of FT-IR, XRD, and SEM/EDX images taken before and after dye loading showed that the adsorption mechanisms of TB, CV, and RB on the LDAC physically occur. The pseudo-second-order kinetic model better described the adsorption behavior of TB, CV, and RB on the LDAC. The boundary layer thickness value for all the dyes studied increased with increasing initial dye concentration and temperature, and CV also had a larger boundary layer thickness value than that of TB and RB.

Keywords: dye; wastewater remediation; kinetic; thermodynamic.

INTRODUCTION

Today, water pollution has become a very important problem all over the world. One of the main causes of water pollution is industrialization. For example, it is estimated that approximately 25 % of the pollution of the world's clean waters comes from dyeing and finishing processes in the textile industry. Water consumption for dyeing 1 kg of textile products can vary from approximately 25 L kg⁻¹ to 280 L kg⁻¹, and process wastewater can reach 120 L kg⁻¹. Many process wastewaters include dyes such as TB, CV, and RB, which are widely used in different industries such as textiles, leather, paints, food, plastic, paper, and etc.¹ The release of these dyes from industrial wastewater into the environment causes

*Corresponding author e-mail: hulya.koyuncu@btu.edu.tr
<https://doi.org/10.2298/JSC23053089K>

a very serious threat to both human and animal life since they are carcinogenic and non-biodegradable, and even very small amounts can be highly toxic.² In addition, due to the complex chemical structures and long half-lives of these dyes, their persistence in the environment poses a serious danger to the ecosystem (Table S-I). TB, CV, and RB are toxic dyes. These can affect some organs that play an important role in the vital activities of living things and can cause serious problems when exposed, even in very small amounts.³⁻⁶ Due to the harmful effects of TB, CV, and RB, studies are continuing on their removal from water and wastewater. For the removal of dyes from wastewater, there are many different methods, such as adsorption, chemical precipitation, oxidation or ozonation, membrane separation, coagulation or flocculation, biological treatment, and photocatalytic degradation.⁷⁻¹⁸ Most of these methods are expensive, whereas the adsorption method is cheap and has an easy operating procedure. In addition, high efficiency can be obtained. Since commercial activated carbons are expensive, in recent years, researchers have focused on producing activated carbon from sustainable and cheap alternative sources such as agricultural waste, some plants, and fruit peels. Lichen is a symbiotic partnership in which a fungus (mycobiont) and algae and cyanobacteria (photobiont) come together to form a single thallus, with more than 20,000 species found almost everywhere in the world. Although lichens are eco-friendly, sustainable, and low-cost resources, as far as we know, there are very few studies in the literature on the production and use of activated carbon from lichen species.^{19,20}

In this study, it is an innovative approach to use activated carbon synthesized from *Pseudevernia furfuracea* lichen, a common lichen species in the world, to clean water contaminated with toxic dyes such as TB, CV, and RB. Kinetic, equilibrium, and thermodynamic studies were carried out to prove the effectiveness of the innovative adsorbent and demonstrate the adsorption behavior of TB, CV, and RB dyes on the LDAC. Important parameters of the adsorption processes, such as initial concentration, temperature, and time, were optimized through batch-type experiments. Additionally, the reusability of the adsorbent was also studied.

EXPERIMENTAL

Materials

TB (CAS 76-61-9, 1081760025), CV (CAS 548-62-9, 1159400025), and RB (CAS 81-88-9, 1075990025) were purchased from Merck. Some specifications of TB, CV, and RB were shown in Table S-I. For the stock solutions of dyes, certain amounts of CV and RB were dissolved in bi-distilled water, and certain amounts of TB were dissolved in 95 % ethanol. The required initial solution concentrations of TB (20, 40, 60, 80, 100, and 120 mg L⁻¹), CV (15, 30, 45, 60, 75, and 90 mg L⁻¹), and RB (20, 40, 60, 80, 100, and 120 mg L⁻¹) used for the adsorption experiments were prepared from the stock solution by diluting with bi-distilled water.

The activated carbon (LDAC) was synthesized in accordance with our previous report.¹⁹ Preparation and characterization ((Brauner-Emmett-Teller (BET), X-Ray Diffraction (XRD),

Thermogravimetric Analysis (TGA), Fourier Transform Infrared Spectrophotometer (FT-IR) and Scanning Electron Microscope (SEM)) details and the results of the point of zero charge (pH_{PZC}) of the lichen *Pseudevernia furfuracea* and LDAC (Fig. S-1) were already given in our previous study.¹⁹ In this study, contact angle measurement of the LDAC was performed with Attension /Theta Lite. The static sessile drop method was carried out with water. The LDAC powders were pressed into a plate with a hydraulic press (Manuel MSE LP/M2S10).

Adsorption experiments

500 mL of different initial concentrations of TB, CV, and RB dye solutions were mixed with 0.5 g of LDAC and shaken on a shaker (Thermal H11960) for 100 minutes at different temperatures (298 K, 308 K, and 323 K). The pH of the solutions was kept constant at 9.5 in all experiments by adding 0.1 N NaOH and 0.1 N HCl solutions. The samples were centrifuged at 5000 rpm after adsorption, and the filtrates were analyzed by a UV-VIS spectrophotometer (PG Instruments Ltd.). The dye concentrations in the solutions taken at certain times (5, 10, 15, 20, 25, 30, 35, 40, 45, 50, 55, 60, 70, 80, 90, and 100 min) were measured at their highest absorbance wavelengths (TB: 594 nm, CV: 590 nm, and RB: 554 nm). All the experiments were carried out in duplicate under the same conditions, and the average of the obtained data was used as the result.

Equations

The following equations (1 and 2) were used to calculate the removal percentage (%) and adsorption capacity of the dyes:

$$\text{Removal (\%)} = \frac{C_0 - C_t}{C_t} \times 100 \quad (1)$$

$$q_e = \frac{(C_0 - C_e)}{m} \times V \quad (2)$$

C_e , C_t , and C_0 (mg L^{-1}) represented the equilibrium, any time, and the initial concentration of dye, respectively; m (g) represents the mass of the LDAC; and V (L) represents the volume of the solution.

In order to explain the adsorption behavior of the three dyes on the LDAC and to compare them with each other, kinetic and isotherm modeling studies were carried out with the data obtained from experimental studies, and important thermodynamic parameters such as Gibbs free energy (ΔG^0), enthalpy change (ΔH^0), and entropy change (ΔS^0) were also calculated. Pseudo-first-order (PFO), pseudo-second-order (PSO), and intra-particle diffusion (IDM) models were used for kinetic modeling. Langmuir, Freundlich, and D-R models were applied for isotherm modeling. The linearized versions of these models were given in Table S-II.

The adsorption activation energies of TB, CV, and RB dyes on the LDAC were calculated using the linearized version of the Arrhenius equation.

$$\ln(k) = \ln(A) - \frac{E_a}{(RT)} \quad (3)$$

In order to determine whether the adsorption of the dyes studied on the LDAC is favorable or not, the separation factor R_L values were calculated from the following equation:

$$R_L = \frac{1}{(1 + KC_0)} \quad (4)$$

To determine the heat changes during the adsorption of TB, CV, and RB dyes on the LDAC, thermodynamic parameters such as Gibbs free energy (ΔG^0), the enthalpy change (ΔH^0), and entropy change (ΔS^0) were calculated by the following equations:

$$\Delta G^0 = -RT \ln K \quad (5)$$

$$K = \frac{q_e}{C_e} \quad (6)$$

$$\ln K = \frac{\Delta S^0}{R} - \frac{\Delta H^0}{RT} \quad (7)$$

Nonlinear regression Root Mean Squared Error (RMSE) values were calculated to determine which model better fit the experimental data.

$$RMSE = \sqrt{\sum(q_{e,exp} - q_{e,cal})^2 / N} \quad (8)$$

RESULTS AND DISCUSSION

Characterization of the LDAC before and after TB, CV, and RB loading

To determine the LDAC's wettability, contact angle measurements were conducted by the sessile drop method. A contact angle value of less than 90° will generally indicate that it is very convenient to wet the surface and that the water will spread well over the surface. For contact angle values greater than 90°, surface wetting is generally unfavorable, and the water takes the form of a liquid droplet that minimizes contact with the surface. In fact, our previous study demonstrated the efficacy of this adsorbent in removing methylene blue dye.¹⁹ However, the contact angle value of the LDAC could not be given in that study. In this study, the contact angle of the LDAC was measured as 46.90° ± 4.38 (Fig. S-2), providing additional evidence of the good wettability of the LDAC, which is important in the adsorption process.

It was shown in our previous study that the LDAC had a large BET-specific surface area of 851.24 m² g⁻¹.¹⁹ The surface properties of the LDAC before and after TB, CV, and RB adsorption were investigated by SEM/EDX (Fig. S-3). When the surface of LDAC was examined, it was seen that it had a granular and porous form (Fig. S-3.a). Since these pores in the LDAC structure increased the surface area and the number of active centers, it facilitated the adsorption of the studied dyes in a good way (Fig. S-3.b, c, d). The elemental analysis of the LDAC's surface before and after TB, CV, and RB loading was performed by EDX analysis (Fig. S-3.e, f, g, h). Before the adsorption of TB, CV, and RB, the elemental composition of the LDAC was 82.36 % C, 5.66 % O, 6.87 % Cl, and 5.11 % Zn by weight (Fig. S-3.e). The zinc and chlorine in the EDX results are due to ZnCl₂ used in the chemical activation of activated carbon. Since TB, CV, and RB molecules fully occupied all the pores and surface of the LDAC, the elemental composition of the surface (%) changed significantly after TB (C₂₇H₃₀O₅S), CV (C₂₅H₃₀ClN₃), and RB (C₂₈H₃₁ClN₂O₃) adsorption (Fig. S-3.f, g, h).

The FT-IR spectrums of the LDAC before and after TB, CV, and RB adsorption were given in Fig. S-4. The low intensity peaks around 2927-2853 cm⁻¹ show asymmetric and symmetrical aliphatic C-H stretching bands (Fig. S-4).^{4,19} The broad band stretching between 1550 and 1750 cm⁻¹ is likely the result of the

C=N, C=C, and conjugated carbonyl vibrations in the aromatic ring.^{7,19} After the adsorption of TB, CV, and RB on the LDAC, decreases in peak intensities were observed, indicating that adsorption had taken place, although no significant shift was observed in the peaks.

The XRD patterns of the LDAC before and after TB, CV, and RB adsorption were shown in Fig. S-5. As seen in Fig. S-5, there are both sharp peaks and wide peaks in the XRD patterns of the LDAC. Although sharp peaks indicate the presence of crystal structures, broad peaks indicate the presence of amorphous structures. The broad peaks at the 2 theta value of around 25° and 43° in the XRD patterns indicate the existence of amorphous carbonaceous structures. The sharp peaks at $2\theta = 31.5^\circ$, 34.5° , and 36.5° are crystalline carbon structures. It can be said that in the carbonization processes carried out at high temperatures (approximately 800 °C), more crystalline carbon structures, such as graphite, are formed than amorphous structures. In addition, the zinc oxide (from ZnCl₂ activation) trapped in the melt by sintering at high temperatures may not have been sufficiently removed by washing processes. The peaks at $2\theta = 47.4^\circ$ and 56.4° suggest the presence of ZnO. Also, the peaks at $2\theta = 62.7^\circ$ and 67.8° may be due to other impurities. The absence of a significant shift in the peaks after the adsorption of TB, CV, and RB dyes can be explained by the fact that the studied dyes do not form chemical bonds that may cause a change in the structure of the active centers on the LDAC surface (Fig. S-4 and Fig. S-5). In other words, the adsorption took place by physical mechanisms for all the studied dyes.

The effect of some parameters on TB, CV, and RB adsorptions

To compare the adsorption capacities, the removal of TB, CV, and RB from the aqueous medium by the LDAC was investigated at the same pH (9.5). Since this pH value (9.5) was greater than the pH_{pzc} value of the LDAC (6.8) and the pK_a values of the dyes (TB = 8.9, CV = 9.4, and RB = 3.7), the electrostatic attraction force between the dyes and the LDAC was increased. Fig. 1a shows how temperature affects the adsorption of the studied dyes. It is seen that the adsorption capacity (q_e) of all dyes studied increases with increasing temperature. Moreover, the same effect was observed for all initial concentration values. While the q_e values at 298 K were 45.34 mg g⁻¹, 41.41 mg g⁻¹, and 44.67 mg g⁻¹ for TB, CV, and RB, respectively, these values were 51.83 mg g⁻¹, 47.41 mg g⁻¹, and 49.64 mg g⁻¹ at 323 K (60 mg L⁻¹ initial dye concentration). Increasing the temperature increases the mobility of the molecules in the solution medium, decreases the solution viscosity, and helps the expansion of small pores. In addition, the increase in temperature increases the diffusion rate as the external and internal mass transfer resistances decrease. Thus, the transition of molecules from the liquid phase to the solid phase becomes easier. Fig. 1b shows the effect of initial dye concentration (for TB: 20, 40, 60, 80, 100, 120 mg L⁻¹; CV: 15, 30, 45, 60, 75, 90 mg L⁻¹; and RB: 20, 40, 60, 80, 100, 120 mg L⁻¹) on the adsorption capacity (q_e). It appears that

increasing the initial dye concentrations increases the adsorption capacity (q_e) by generating a higher driving force of concentration difference that can overcome the solid-liquid mass transfer resistance. q_e increased with increasing initial concentration at three different temperatures (298 K, 308 K, and 323 K) for the three dyes. The best results were obtained at 323 K. The contact time, of course, directly affects the cost of the adsorption process. Obtaining the highest adsorption efficiency in a shorter time is advantageous for the process. The ability of LDAC to remove TB, CV, and RB from water with high adsorption efficiency in short equilibrium times (90 min, 80 min, and 70 min for TB, CV, and RB, respectively) shows that this adsorbent can reduce the total process cost of removing dyes from contaminated water.

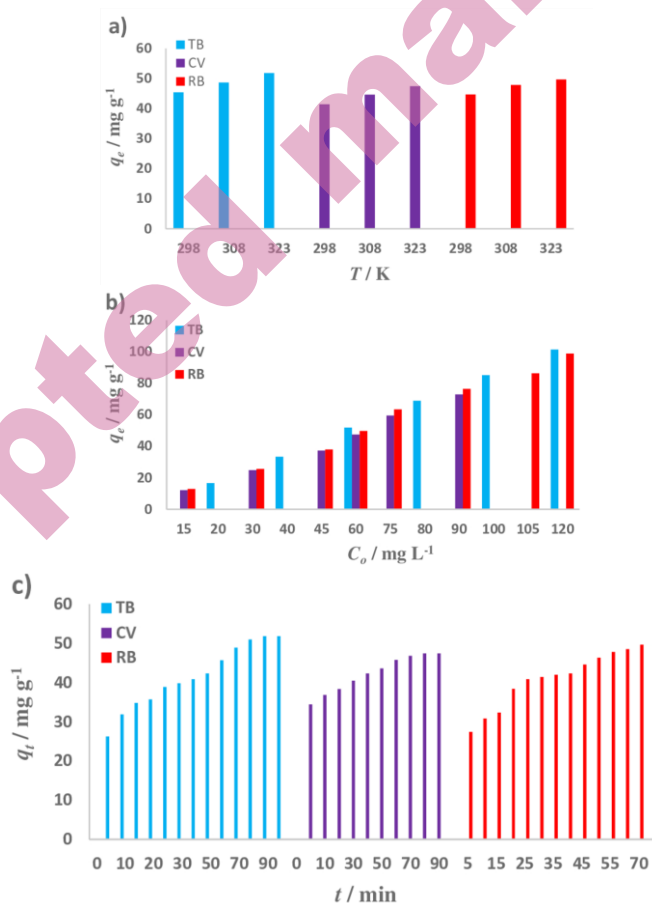


Fig. 1. a) The temperature effects; b) The initial concentration effects; c) The contact time effects.

Fig. 1c shows the effect of contact time on the adsorption capacity (q_e). When the change in the bar graphs is examined, it is seen that there is rapid adsorption due to the high solution concentration in the initial times, then the solution concentration decreases and the adsorption rate decreases with the filling of the active centers on the LDAC surface, and finally, at the end of a certain time, adsorption cannot be made, that is, the equilibrium state is reached.

TB, CV, and RB adsorption kinetics

The adsorption kinetic studies are very important for the modeling and design parameters of the adsorption systems. Three different kinetic models were applied to the experimental data to estimate the adsorption rates and determine the rate-limiting step, and linear forms of the PFO, PSO, and IDM models were used to determine the model parameters (Table I). In addition, nonlinear forms of PFO, PSO, and IDM models were applied to the experimental data, and experimental kinetic data were also checked (Fig. 2).

PFO model parameters (k_1 , q_e), correlation coefficient (R^2), deviation (%) between calculated q_e and experimental q_e values, and *RMSE* values calculated at 323 K temperature for the three dyes studied were given in Table I. The fact that the R^2 values were lower, the deviation (%) and *RMSE* values were higher than the other two models examined showed that this model did not fit the experimental data. Furthermore, Fig. 2 proved that the experimental kinetic data did not fit the nonlinear form of the PFO model at all for TB, CV, and RB.

Table I. PFO, PSO, and IDM model parameters for the adsorption of TB, CV, and RB

Model	Parameters	TB	CV	RB
PFO	$q_{e,exp} / \text{mg g}^{-1}$	51.83	47.41	49.64
	k_1 / min^{-1}	0.0364	0.0420	0.0488
	$q_{e,cal} / \text{mg g}^{-1}$	32.86	19.36	32.54
	R^2	0.8752	0.9077	0.9276
	Deviation / %	36.60	59.16	34.45
	<i>RMSE</i>	17.85	27.41	16.50
PSO	$k_2 / \text{g mg}^{-1} \text{min}^{-1}$	0.00172	0.00419	0.00213
	$k_0 / \text{g mg}^{-1} \text{min}^{-1}$	5.4318	10.2774	6.3492
	$q_{e,cal} / \text{mg g}^{-1}$	50.39	46.69	48.66
	R^2	0.9915	0.9970	0.9944
	Deviation / %	2.78	1.52	1.97
IDM	<i>RMSE</i>	1.37	0.81	0.62
	$k_d / \text{mg g}^{-1} \text{min}^{-1/2}$	3.1800	1.8903	3.5112
	$\theta / \text{mg g}^{-1}$	21.576	30.383	20.840
	R^2	0.9802	0.9880	0.9577
	$q_{e,cal} / \text{mg g}^{-1}$	51.74	47.29	50.22
IDM	Deviation / %	0.17	0.25	1.17
	<i>RMSE</i>	0.91	0.60	1.32

PSO model parameters (k_2 , q_e) and the initial adsorption rate (k_0), R^2 , deviations (%), and $RMSE$ values calculated for TB, CV, and RB were given in Table I. R^2 values were greater than 0.99 for all dyes studied. The smaller deviation (%) values indicating good closeness between experimental q_e and calculated q_e were found to be 2.78, 1.52, and 1.97 for TB, CV, and RB, respectively. The smaller $RMSE$ values (1.37, 0.81, and 0.62 for TB, CV, and RB, respectively) supported the fact that the adsorption of TB, CV, and RB on the LDAC follows the PSO kinetics well. In addition, the rate constant (k_2) and the initial adsorption rate (k_0) of TB were greater than those of RB and CV, indicating that the affinity of TB molecules for the LDAC is greater than that of CV and RB molecules (Table I). Moreover, Fig. 2 demonstrated that the experimental kinetic data for TB, CV, and RB fit well with the nonlinear form of the PSO model. Bakhsh *et al.* reported that the adsorption of thymol blue onto prepared activated carbon from *Trachycarpus fortunei* seeds obeyed the pseudo-second-order model.²¹ Senthilkumaar *et al.* reported that the kinetics of adsorption of crystal violet onto modified activated carbons prepared from male flowers of coconut trees were found to be pseudo-second-order with regard to intraparticle diffusion.²² Wang *et al.* reported that the adsorption of Rhodamine B on biochar samples prepared from earthworm manure fitted well with the PSO kinetic model.²³

IDM model parameters (k_d , θ), R^2 , deviations (%), and $RMSE$ values calculated for the three dyes studied were given in Table I. The fact that the q_t vs. $t^{1/2}$ graphs did not pass through the origin indicated that the mass transfer rate changed in the first and last stages of adsorption. This suggests that intraparticle diffusion is not the only step controlling the rate, and boundary layer effects can also control the rate of adsorption.

The θ parameter is very important as it relates to the boundary layer thickness. The bigger the θ value, the larger the boundary layer thickness. The values of the boundary layer thickness for TB, CV, and RB were calculated as 21.576 mg g⁻¹, 30.383 mg g⁻¹, and 20.840 mg g⁻¹, respectively (Table I). In addition, the boundary layer thickness values for all studied dyes increased with increasing initial dye concentration and temperature. The greater boundary layer thickness value of CV may explain why the adsorption capacity of CV on LDAC is lower than that of TB and RB. This indicates that intra-particle diffusion was slower at higher temperatures and initial dye concentrations. The rate constants (k_d) for TB, CV, and RB were found to be 3.1800 mg g⁻¹ min^{-1/2}, 1.8903 mg g⁻¹ min^{-1/2}, and 3.5112 mg g⁻¹ min^{-1/2} at 323 K, respectively (Table I). The R^2 , deviations (%), and $RMSE$ values for the IDM model show that the IDM kinetic model is suitable for the studied dyes. The lower deviation (%) and $RMSE$ values of TB and CV compared to RB indicate a better fit. As can be seen from Fig. 2, the nonlinear form of the IDM model is in good agreement with the experimental kinetic data for TB, CV,

and RB, suggesting that both pore and film diffusion co-control the adsorption kinetics.

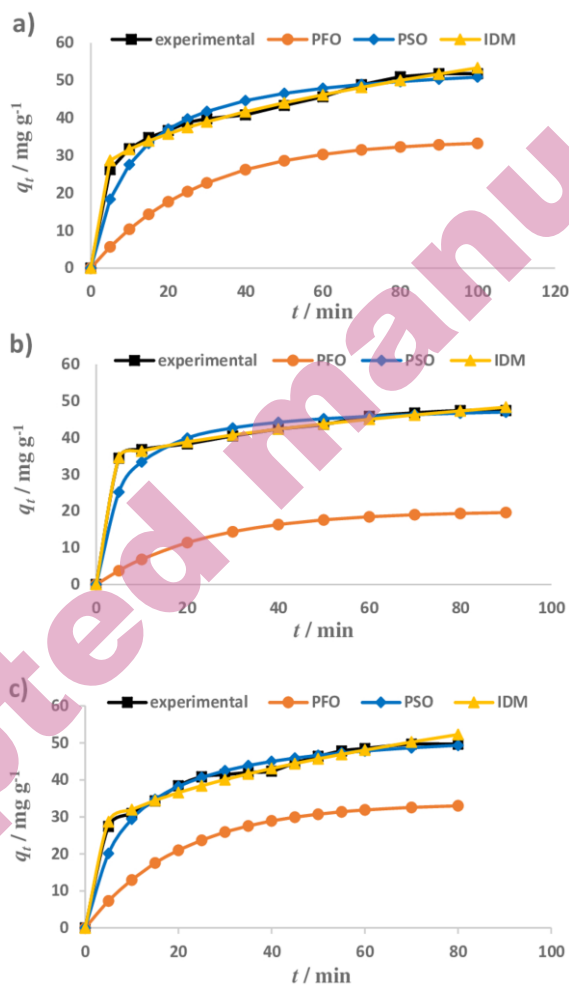


Fig. 2. a) The kinetic modeling of TB; b) The kinetic modeling of CV; c) The kinetic modeling of RB.

Activation energy

The activation energy offers an idea about whether the adsorption mechanism is physical or chemical. If the activation energy is less than 40 kJ mol⁻¹, it is physical adsorption; if it is greater than 40 kJ mol⁻¹, it is chemical adsorption. For the adsorption of TB, CV, and RB onto LDAC, the activation energies (E_a) were calculated using eq. (3) and the Arrhenius plots (Figs. not given). The activation energies were found to be 45.41 kJ mol⁻¹, 20.51 kJ mol⁻¹, and 27.04 kJ mol⁻¹ for

TB, CV, and RB, respectively. Although the activation energy of TB is slightly higher than 40 kJ mol^{-1} , the energy value (E) determined from the D-R model and the absence of significant shifts in the FT-IR and XRD images suggest that the adsorption is physical. Onen *et al.* reported that the activation energy of TB on mild steel was 6.32 kJ mol^{-1} .²⁴ Laskar and Kumar noted that the value of E_a for crystal violet dye adsorption onto sodium carbonate-modified Bambusa tulda was $26.297 \text{ kJ mol}^{-1}$.²⁵ Lee and Zaini reported that the activation energy for the adsorption of RB by magnetic activated carbon was 24.1 kJ mol^{-1} and 28.9 kJ mol^{-1} for the PFO and PSO kinetic models, respectively.²⁶

TB, CV, and RB adsorption isotherms

Equilibrium studies are necessary in order to optimize the adsorption process. The equilibrium studies of the adsorption process of TB, CV, and RB dyes on LDAC were carried out at 3 different temperatures (298 K, 308 K, and 323K), and the experimental data were adapted to 3 different isotherm models (Langmuir, Freundlich, and D-R), and the determined model parameters were presented in Table II.

The maximum Langmuir adsorption capacity (q_m) of TB, CV, and RB was found to be 400 mg g^{-1} , $212.766 \text{ mg g}^{-1}$, and $344.828 \text{ mg g}^{-1}$, respectively (Fig. S-6a). The value of q_m for TB is higher than that of CV and RB. The reason for this can be explained by the fact that the initial rate of adsorption (k_0) for TB acquired from the PSO model is lower than that of CV and RB. So, TB molecules are adsorbed on the LDAC surface faster. Besides, the smaller boundary layer thickness (θ) of TB allows the molecules to pass easily into the pores of the LDAC (Table I). Kumari *et al.* studied the adsorption of TB dye from wastewater by activated carbons fabricated from plastic waste and reported that the maximum adsorption capacities onto waste polybags (P-ACs), cups (C-ACs), and bottles (B-ACs) were 16.28 mg g^{-1} , 115.4 mg g^{-1} , and 43.93 mg g^{-1} , respectively.²⁷ Senthilkumaar *et al.* reported that the adsorption capacities of CV onto activated carbons (PAAC and SAAC) derived from male flowers of coconut trees were 60.42 mg g^{-1} and 85.84 mg g^{-1} .²² Xiao *et al.* found the maximum adsorption capacity of RB onto activated carbon (ASC) was 123.46 mg g^{-1} .²⁸ It can be stated that the maximum adsorption capacity (q_m) of TB, CV, and RB onto the LDAC obtained in this study is relatively higher than many adsorbent capacities reported by other researchers. In addition, the favorable adsorption of TB, CV, and RB on LDAC was demonstrated by the R_L factor being in the range of 0 to 1 (Table II). Similar results regarding the R_L factor of TB, CV, and RB on different adsorbents were obtained by the other authors.^{22,28,29}

The Freundlich model parameters (k_f , n) and R^2 values for the studied dyes were given in Table II. k_f values were determined as 9.6244, 4.8018, and 6.7113 for TB, CV, and RB, respectively (Fig. S-6b). If the k_f value is large, the adsorption capacity is also large. By comparing the k_f values for the studied dyes in Table II,

it can be said that the adsorption capacity of LDAC is ranked as TB>RB>CV. If the value of n is greater than 1, it is favorable adsorption. n values were found to be greater than 1 for the removal of TB, CV, and RB (Table II). Besides, $n > 1$ indicates high affinity between the LDAC and TB, CV, and RB and proves that the adsorption occurs in a physical manner and that the adsorption sites on the LDAC are heterogeneous. Other researchers revealed similar results related to the favorable adsorption of TB, CV, and RB onto different adsorbents.^{27,29,30}

The R^2 values for Langmuir, Freundlich, and D-R isotherms were determined to be greater than 0.99 for both TB and RB and greater than 0.97 for CV.

Table II. Langmuir, Freundlich, and D-R parameters for the adsorption of TB, CV, and RB

	TB	CV	RB
<u>Langmuir</u>			
$q_m / \text{mg g}^{-1}$	400	212.766	344.828
$K / \text{L mg}^{-1}$	0.0183	0.0260	0.0182
R^2	0.9991	0.9797	0.9977
R_L	0.4766	0.3903	0.4772
<u>Freundlich</u>			
k_f	9.6244	4.8018	6.7113
n	1.2384	1.0611	1.1227
R^2	0.9976	0.9749	0.9919
<u>D-R</u>			
$q_m / \text{mol g}^{-1}$	0.0383	0.0136	0.0114
$K' / \text{mol}^2 \text{kJ}^{-2}$	0.0081	0.0070	0.0065
$E / \text{kJ mol}^{-1}$	7.8567	8.4515	8.7706
R^2	0.9850	0.9788	0.9921

The adaptation of the experimental data to the D-R model was shown in Fig. S-6c and the calculated D-R parameters (q_m , K' , and E) and R^2 values were given in Table II. The E value calculated from the D-R model indicates that when $E < 8 \text{ kJ mol}^{-1}$, the adsorption mechanism is physical, when $8 < E < 16 \text{ kJ mol}^{-1}$, it is ion exchange adsorption, and when $E > 16 \text{ kJ mol}^{-1}$, the adsorption is chemical. In this study, E values were calculated to be $7.8567 \text{ kJ mol}^{-1}$, $8.4515 \text{ kJ mol}^{-1}$, and $8.7706 \text{ kJ mol}^{-1}$ for TB, CV, and RB, respectively (Table II). The type of adsorption of TB on the LDAC was of a physisorption nature. In other words, the interaction between TB molecules and LDAC takes place by van der Waals forces. Although the values of E for CV and RB seem to be in the ion exchange range, they are very close to 8 kJ mol^{-1} , and it can be stated that the interaction between both CV and RB molecules and the LDAC surface is also by physical adsorption mechanisms.

A comparison of the maximum adsorption capacity of the LDAC with various activated carbons used as cheap adsorbents for TB, CV, and RB removal was given in Table III. This comparison demonstrated that the LDAC had a greater adsorption capacity than other adsorbents. Thus, the LDAC can be considered an adsorbent

with great potential to remove dyes such as TB, CV, and RB from aqueous medium.

Table III. Comparison between LDAC and cheap biomass-based activated carbons for TB, CV, and RB removal

Activated carbon	TB / mg g ⁻¹	CV / mg g ⁻¹	RB / mg g ⁻¹	Ref.
<i>Garcinia cola</i> nut shell (CBK1/1)	189.60			29
<i>Garcinia cola</i> nut shell (CBH2/1)	396.04			29
Plastic waste polybags (P-ACs)	16.28			27
Plastic waste cups (C-ACs)	115.40			27
Plastic waste bottles (B-ACs)	43.93			27
Coconut tree male flowers (PAAC)		60.42		22
Coconut tree male flowers (SAAC)		85.84		22
<i>Millettia thonningii</i> seed pods-derived		7.57		30
Palm petiole-derived		209		31
Oak leaves-derived		41.15		32
Activated sugar-based carbon (ASC)			123.46	28
Earthworm manure-derived			21.60	23
Bamboo shoot shell-derived			85.8	33
Plantain peels-derived			84.41	34
Cassava slag-derived			105.6	35
LDAC	400	212.77	344.83	Present study

Adsorption thermodynamics

Thermodynamic parameters of the adsorption of TB, CV, and RB on the LDAC, such as the Gibbs free energy (ΔG^0 / kJ mol⁻¹), enthalpy (ΔH^0 / kJ mol⁻¹), and entropy (ΔS^0 / kJ mol⁻¹ K⁻¹) changes, were calculated using Eqs. (5-7) and the van't Hoff plot (Fig. S-7), and the results were shown in Table IV. The negative values of ΔG^0 showed that TB, CV, and RB adsorption on the LDAC was spontaneous and feasible (Table IV). The positive values of ΔH^0 indicated endothermic adsorption. The ΔH^0 values for CV and RB are less than 20 kJ mol⁻¹ (Table IV), indicating physical adsorption by van der Waals forces. Although the ΔH^0 value for TB is slightly higher than 20 kJ mol⁻¹, it can be said that the interaction between TB and the LDAC occurs physically with electrostatic forces. Moreover, the calculated activation energy and D-R energy values for TB, CV, and RB support these thermodynamic results. The increase in randomness and

disorder at the dye solution-LDAC interface during the adsorption was designated by positive values of ΔS^0 , which is in accordance with the 2nd law of thermodynamics. Similar results for TB, CV, and RB adsorption on different activated carbons have been reported by other researchers.^{29,31,35}

Table IV. The values of thermodynamic parameters (60 ppm, 323 K)

	K	$\Delta G^0 / \text{kJ mol}^{-1}$	$\Delta H^0 / \text{kJ mol}^{-1}$	$\Delta S^0 / \text{kJ mol}^{-1} \text{K}^{-1}$	R^2
TB	6.3439	-4.8845	22.9192	0.0864	0.9987
CV	3.7657	-3.5056	16.6537	0.0627	0.9904
RB	4.7915	-4.1425	17.7545	0.0748	0.8293

Reusability

The reusability of the LDAC was evaluated for TB, CV, and RB adsorption and desorption, and results were shown in Fig. S-8. 0.1 M HCl solution was used for the desorption studies. After four consecutive adsorption and desorption cycles, the removal efficiencies of TB, CV, and RB decreased by 23.5 %, 19.1 %, and 15.4 %, respectively. This demonstrated that LDAC could be an economical and effective adsorbent for dye removal.

CONCLUSIONS

The adsorption behaviors of TB, CV, and RB on LDAC were studied, and very good results were achieved. The isotherm studies showed that the adsorption capacity of the LDAC was ranked as TB > RB > CV. The maximal Langmuir adsorption capacity of TB, CV, and RB was found as 400 mg g⁻¹, 212.766 mg g⁻¹, and 344.828 mg g⁻¹, respectively. The kinetic studies implied that the adsorption of TB, CV, and RB onto the LDAC fit the PSO kinetics. Besides, the nonlinear forms of the PSO and IDM models had a good agreement with the experimental kinetic data for TB, CV, and RB. The boundary layer thicknesses were also evaluated. These values for TB, CV, and RB were calculated to be 21.576 mg g⁻¹, 30.383 mg g⁻¹, and 20.840 mg g⁻¹, respectively. TB and CV better fit the IDM kinetic model with lower deviation (%) and RMSE values compared to RB. The thermodynamic studies showed that the adsorption of TB, CV, and RB on the LDAC was spontaneous, feasible, and endothermic, with physical adsorption by van der Waals and electrostatic forces.

This study demonstrated that the removal of the dyes with environmentally friendly, cheap, sustainable, and high adsorption capacity the LDAC will contribute to environmental and wastewater cleaning, and it may be an alternative to expensive adsorbents.

SUPPLEMENTARY MATERIAL

Additional data are available electronically at the pages of journal website: <https://www.shd-pub.org.rs/index.php/JSCS/article/view/12417>, or from the corresponding author on request.

ИЗВОД

ИСТРАЖИВАЊЕ ПОНАШАЊА АДСОРПЦИЈЕ ТИМОЛ ПЛAVОГ, КРИСТАЛНО ЛУБИЧАСТОГ И РОДАМИНА Б НА АКТИВНОМ УГЉУ ДОБИЈЕНОМ ОД ЛИШАЈА

HÜLYA KOYUNCU¹, ALİ RIZA KUL²

¹Bursa Technical University, Faculty of Engineering and Natural Sciences, Chemical Engineering Department, 16310, Bursa, Turkiye, and ²Van Yüzüncü Yıl University, Faculty of Science, Chemistry Department, 65080, Van, Turkiye.

Пошто се тимол плава (ТВ), кристално љубичаста (CV) и родамин б (RB) често користе у разним индустријама, они узрокују загађење животне средине услед процесних отпадних вода. Садашња студија се фокусира на уклањање ТВ, CV и RB из водених медија помоћу активног угља добијеног од лишља (LDAC), и упоређивање њиховог понашања при адсорпцији. Утврђено је да је максимални капацитет Лангмуир адсорпције за ТВ, CV и RB 400 mg g^{-1} , $212,766 \text{ mg g}^{-1}$ и $344,828 \text{ mg g}^{-1}$, респективно. Нађено је да уклањање ТВ, CV и RB износи 86,38 %, 79,02 % и 82,73 %, респективно, при истим условима. Експериментални подаци су интерпретирани уобичајено коришћеним кинетичким и изотермним моделима. Израчунате енергије активације, енергија D-R модела, вредности енталпије и процена FT-IR, XRD и SEM/EDX слика снимљених пре и после адсорпције боје показали су да се механизми адсорпције ТВ, CV и RB на LDAC физички процеси. Кинетички модел псеудо-другог реда боље је описао адсорпционо понашање ТВ, CV и RB на LDAC-у. Вредност дебљине граничног слоја за све проучаване боје повећавала се са повећањем почетне концентрације боје и температуре, а CV је такође имао већу вредност дебљине граничног слоја од оне која је нађена код ТВ и RB.

(Примљено 30. маја; ревидирано 10. августа; прихваћено 20. новембра 2023.)

REFERENCES

1. C. Puri, G. Sumana, *Appl. Clay Sci.* **166** (2018) 102–112 (<https://doi.org/10.1016/j.clay.2018.09.012>)
2. M. Sh. Gohr, A. I. Abd-Elhamid, A. A. El-Shanshory, H. M. A. Soliman, *J. Mol. Liq.* **346** (2022) 118227 (<https://doi.org/10.1016/j.molliq.2021.118227>)
3. S. Kumar (S. Kumar), R. D. Kaushik, L. P. Purohit, *J. Hazard. Mater.* **424** (2022) 127332 (<https://doi.org/10.1016/j.jhazmat.2021.127332>)
4. P. Naderi, M. Shirani, A. Semnani, A. Goli, *Ecotoxicol. Environ. Saf.* **163** (2018) 372–381 (<https://doi.org/10.1016/j.ecoenv.2018.07.091>)
5. M. El Alouani, S. Alehyen, H. El Hadki, H. Saufi, A. Elhalil, O. K. Kabbaj, M. Taibi, *Surfaces and Interfaces* **24** (2021) 101136 (<https://doi.org/10.1016/j.surfin.2021.101136>)
6. M. Sundararajan, V. Sailaja, L. John Kennedy, J. Judith Vijaya, *Ceram. Int.* **43** (2017) 540–548 (<http://doi.org/10.1016/j.ceramint.2016.09.191>)
7. A. S. Takabi, M. Shirani, A. Semnani, *Environ. Technol. Innov.* **24** (2021) 101947 (<https://doi.org/10.1016/j.eti.2021.101947>)

8. G. Sharma, A. Kumar, M. Naushad, A. García-Peñas, A. H. Al-Muhtaseb, A. A. Ghfar, V. Sharma, T. Ahamad, F. J. Stadler, *Carbohydr. Polym.* **202** (2018) 444–453 (<https://doi.org/10.1016/j.carbpol.2018.09.004>)
9. S. S. Chan, K. S. Khoo, K. W. Chew, T. C. Ling, P. L. Show, *Bioresour. Technol.* **344** (2022) 126159 (<https://doi.org/10.1016/j.biortech.2021.126159>)
10. S. Sathiyavimal, S. Vasantharaj, M. Shanmugavel, E. Manikandan, P. Nguyen-Tri, K. Brindhadevi, A. Pugazhendhi, *Prog. Org. Coatings* **148** (2020) 105890 (<https://doi.org/10.1016/j.porgcoat.2020.105890>)
11. P. V. Nidheesh, R. Gandhimathi, *Desalination* **299** (2012) 1–15 (<https://doi.org/10.1016/j.desal.2012.05.011>)
12. A. Muniyasamy, G. Sivaporul, A. Gopinath, R. Lakshmanan, A. Altaee, A. Achary, P. Velayudhaperumal Chellam, *J. Environ. Manage.* **265** (2020) 110397 (<https://doi.org/10.1016/j.jenvman.2020.110397>)
13. S. Ledakowicz, R. Żyła, K. Paździor, J. Wrębiak, J. Sójka-Ledakowicz, *Ozone Sci. Eng.* **39** (2017) 357–365 (<https://doi.org/10.1080/01919512.2017.1321980>)
14. H. R. Rashidi, N. M. N. Sulaiman, N. A. Hashim, C. R. C. Hassan, M. R. Ramli, *Desalin. Water Treat.* **55** (2015) 86–95 (<https://doi.org/10.1080/19443994.2014.912964>)
15. D. A. Gopakumar, V. Arumukhan, R. V. Gelamo, D. Pasquini, L. C. de Morais, S. Rizal, D. Hermawan, A. Nzihou, H. P. . A. Khalil, *Nano-Structures & Nano-Objects* **18** (2019) 100268 (<https://doi.org/10.1016/j.nanoso.2019.100268>)
16. M. R. Gadekar, M. M. Ahammed, *Desalin. Water Treat.* **57** (2016) 26392–26400 (<https://doi.org/10.1080/19443994.2016.1165150>)
17. H. Zazou, H. Afanga, S. Akhouairi, H. Ouchtak, A. A. Addi, R. A. Akbour, A. Assabbane, J. Douch, A. Elmchaouri, J. Duplay, A. Jada, M. Hamdani, *J. Water Process Eng.* **28** (2019) 214–221 (<https://doi.org/10.1016/j.jwpe.2019.02.006>)
18. S. M. Ghoreishi, R. Haghghi, *Chem. Eng. J.* **95** (2003) 163–169 ([https://doi.org/10.1016/S1385-8947\(03\)00100-1](https://doi.org/10.1016/S1385-8947(03)00100-1))
19. H. Koyuncu, A. R. Kul, *Surfaces and Interfaces* **19** (2020) 100527 (<https://doi.org/10.1016/j.surfin.2020.100527>)
20. H. Koyuncu, A. R. Kul, *Surfaces and Interfaces* **21** (2020) 100653 (<https://doi.org/10.1016/j.surfin.2020.100653>)
21. E. M. Bakhsh, M. Bilal, M. Ali, J. Ali, A. Wahab, K. Akhtar, T. M. Fagieh, E. Y. Danish, A. M. Asiri, S. B. Khan, *Materials (Basel)*. **15** (2022) 1986 (<https://doi.org/10.3390/ma15061986>)
22. S. Senthilkumaar, P. Kalaamani, C. Subburaam, *J. Hazard. Mater.* **136** (2006) 800–808 (<https://doi.org/10.1016/j.jhazmat.2006.01.045>)
23. Z. Wang, D. Shen, F. Shen, C. Wu, S. Gu, *Int. Biodeterior. Biodegradation* **120** (2017) 104–114 (<https://doi.org/10.1016/j.ibiod.2017.01.026>)
24. A. I. Onen, O. N. Maitera, J. Joseph, J. E. E. Ebenso, *Int. J. Electrochem. Sci.* **6** (2011) 2884–2897 (<http://www.electrochemsci.org/papers/vol6/6072884.pdf>)
25. N. Laskar, U. Kumar, *KSCE J. Civ. Eng.* **22** (2018) 2755–2763 (<https://doi.org/10.1007/s12205-017-0473-5>)
26. L. Z. Lee, M. A. Ahmad Zaini, *Toxin Rev.* **41** (2022) 64–81 (<https://doi.org/10.1080/15569543.2020.1837172>)
27. M. Kumari, G. R. Chaudhary, S. Chaudhary, A. Umar, *Chemosphere* **294** (2022) 133692 (<https://doi.org/10.1016/j.chemosphere.2022.133692>)

28. W. Xiao, Z. N. Garba, S. Sun, I. Lawan, L. Wang, M. Lin, Z. Yuan, *J. Clean. Prod.* **253** (2020) 119989 (<https://doi.org/10.1016/j.jclepro.2020.119989>)
29. I.-H. T. Kuete, D. R. T. Tchuifon, G. N. Ndifor-Angwafor, A. T. Kamdem, S. G. Anagho, *J. Encapsulation Adsorpt. Sci.* **10** (2020) 1–27 (<https://doi.org/10.4236/jeas.2020.101001>)
30. E. E. Jasper, V. O. Ajibola, J. C. Onwuka, *Appl. Water Sci.* **10** (2020) 132 (<https://doi.org/10.1007/s13201-020-01218-y>)
31. H.-O. Chahinez, O. Abdelkader, Y. Leila, H. N. Tran, *Environ. Technol. Innov.* **19** (2020) 100872 (<https://doi.org/10.1016/j.eti.2020.100872>)
32. M. Sulyman, J. Namieśnik, A. Gierak, *Polish J. Environ. Stud.* **23** (2014) 2223 (<https://doi.org/10.15244/pjoes/26764>)
33. Y. Hou, G. Huang, J. Li, Q. Yang, S. Huang, J. Cai, *J. Anal. Appl. Pyrolysis* **143** (2019) 104694 (<https://doi.org/10.1016/j.jaap.2019.104694>)
34. F. A. Adekola, S. B. Ayodele, A. A. Inyinbor, *Chem. Data Collect.* **19** (2019) 100170 (<https://doi.org/10.1016/j.cdc.2018.11.012>)
35. J. Wu, J. Yang, G. Huang, C. Xu, B. Lin, *J. Clean. Prod.* **251** (2020) 119717 (<https://doi.org/10.1016/j.jclepro.2019.119717>).